Chinese Chemical Letters 32 (2021) 3071–3075

Contents lists available at ScienceDirect

Chinese Chemical Letters

journal homepage: www.elsevier.com/locate/cclet

Communication

Cocrystallization-like strategy for the codelivery of hydrophobic and hydrophilic drugs in a single carrier material formulation

Yi Li[a,1], Chao Teng[a,1], Helena S. Azevedo[b], Lifang Yin[a,*], Wei He[a,*]

[a] School of Pharmacy, China Pharmaceutical University, Nanjing 210009, China
[b] School of Engineering and Materials Science, Institute of Bioengineering, Queen Mary University of London, London E1 4NS, United Kingdom

ARTICLE INFO

Article history:
Received 6 January 2021
Received in revised form 31 March 2021
Accepted 1 April 2021
Available online 2 April 2021

Keywords:
Hybrid nanocrystal
Codelivery
Multidrug resistance
Paclitaxel
Dichloroacetic acid
Cocrystallization

ABSTRACT

Codelivery of drugs by drug carriers is a promising strategy against several diseases such as infections and cancer. However, traditional drug carriers are typically characterized by low drug payload, limiting their treatment efficacy. Using nanocrystals of insoluble drug as carriers, a carrier free platform was developed previously to deliver a second insoluble drug for codelivery. To extend the concept, we hypothesized, herein, that the platform allows for codelivery of hydrophobic and hydrophilic drugs using a cocrystalization-like strategy. To obtain proof-of-concept, paclitaxel (PTX), an insoluble chemotherapeutic agent, and dichloroacetic acid (DCA), a water-soluble inhibitor of pyruvate dehydrogenase kinase, were utilized as model drugs. PTX-DCA hybrid nanocrystals (PTX-DCA NCs) were prepared by anti-solvent precipitation and characterized. Their *in vitro* antitumor activity against cancer cells was evaluated. PTX-DCA NCs prepared from the optimized formulation had a diameter of 160 nm and a rod-shape morphology and possessed encapsulated efficacy of approximately 30% for DCA. The use of the hybrid crystals enabled synergy to kill cancer cells, in particular in PTX-resistant cells in a dose-dependent pattern. In conclusion, by using a cocrystalization-like strategy, a hydrophilic drug can be formulated into a drug's nanocrystal for codelivery.

Codelivery of two drugs or more is a promising approach for combinatory therapy and treating diseases, due to its benefits such as enhanced therapeutic selectivity, synergy, reduced side effects, and improved patient's compliance [1]. Drug-carrier techniques, encompassing liposomes, polymeric micelles, nanoemulsions, solid lipid nanoparticles, carbon nanotubes, and inorganic particles are commonly used to facilitate drug delivery [2–5]. However, these drug carriers often have low drug-loading capacity, typically less than 10% (w/w) and, as a result, limiting the treatment efficacy [6–8]. Furthermore, the low payload becomes more restrictive in codelivery as multiple drugs are required for loading.

Nanocrystals of insoluble active compounds are nanoscale drug particles [9,10]. Nanocrystals have noticeably high drug loading since the nanocrystal particles are 100% drug [10,11]. Previously, by using drug nanocrystals as carriers, a carrier free platform of codelivery was developed to codeliver insoluble drugs [12,13]. We demonstrated that *via* a cocrystalization-like strategy one drug could be incorporated into the second drug's nanocrystals, forming hybrid drug crystals to improve delivery of the two hydrophobic drugs [12,13]. Herein, we hypothesized that the cocrystalization approach allows for codelivery of insoluble and hydrophilic drugs as well, which the water-soluble drug is formulated inside the crystals of hydrophobic drug.

Paclitaxel (PTX) is a poorly water-soluble chemotherapeutic drug with a water solubility of 0.3 mg/mL [14]. PTX is potent to kill cancer cells and acts *via* destroying the dynamic balance between tubulin and tubulin dimer, and as a result, inhibiting the mitosis of cancer cells and inducing apoptosis [15]. On the other hand, dichloroacetic acid (DCA), a small molecule inhibitor of pyruvate dehydrogenase kinase, enables promoted apoptosis by interfering with glucose metabolism in cancer cells [16]. Recent studies demonstrated that DCA could inhibit stress cell autophagy [17,18] and reverse multi-drug resistance (MDR) by reducing the activity of drug efflux pump on cell membrane [19]. Besides, DCA is also reported to have the function of switching cytoplasmic glucose metabolism to mitochondrial oxidative phosphorylation [20,21]. Consequently, codelivery of the two drugs has potential synergy to poison cancer cells.

To obtain proof-of-concept, we prepared PTX-DCA hybrid nanocrystals (PTX-DCA NCs) *via* anti-solvent precipitation with denatured bovine serum albumin (BSA) as a stabilizer (Fig. 1). To

* Corresponding authors.
E-mail addresses: lifangyin_@163.com (L. Yin), weihe@cpu.edu.cn (W. He).
[1] The authors contributed equally to this work.

https://doi.org/10.1016/j.cclet.2021.03.085
1001-8417/

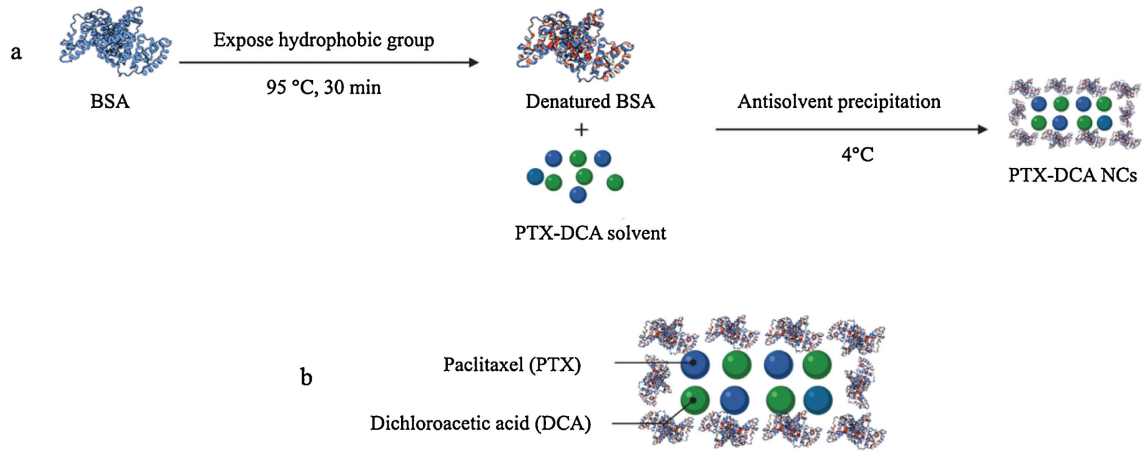

Fig. 1. Scheme illustrating the preparation of PTX-DCA NCs *via* anti-solvent precipitation (a) and PTX-DCA NCs stabilized with BSA (b).

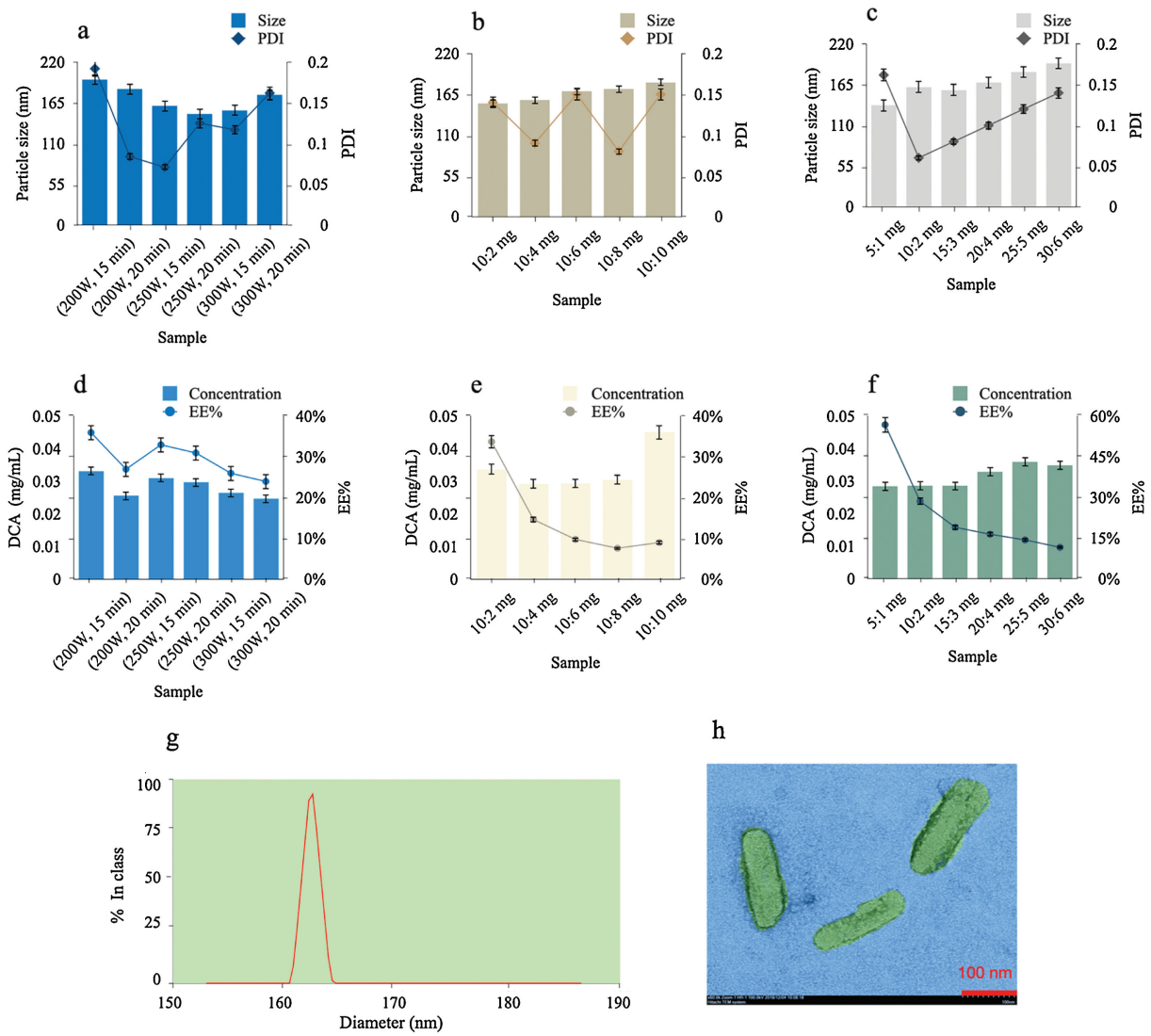

Fig. 2. Preparation and characterization of the hybrid drug nanocrystals. (a-c) Average particle size and PDI, (d-f) EE% of DCA in various formulations of PTX-DCA NCs. (g) Size distribution and (h) TEM image of PTX-DCA NCs prepared from the optimized formulation, involving the use of 10 mg of PTX and 2 mg of DCA, subjected to ultrasonic treatment at a power intensity of 250 W for 15 min.

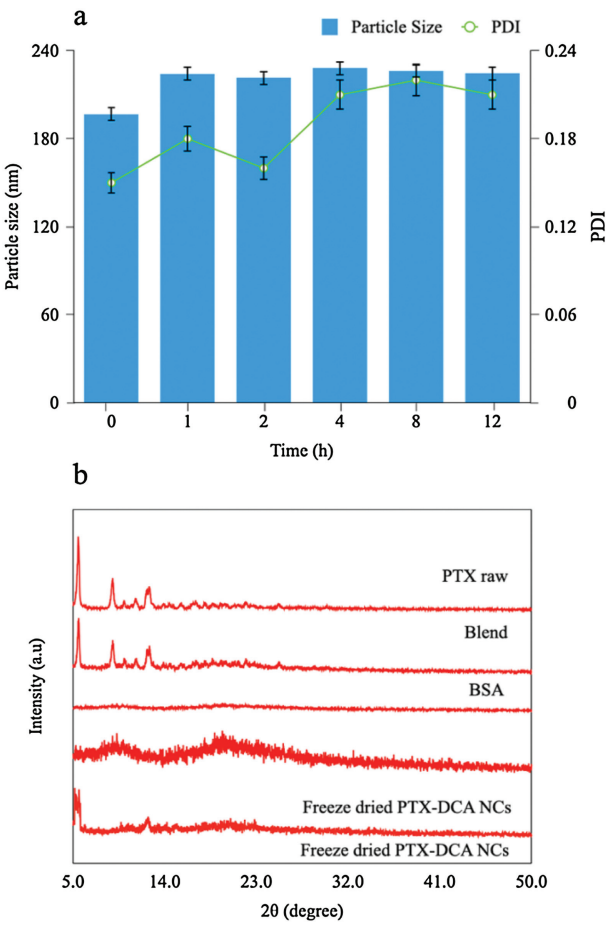

Fig. 3. (a) *In vitro* stability of the NCs after incubation in serum-containing PBS; (b) PXRD characterization.

optimize the formulations, we first tested the influence of ultrasonication conditions on the particle size, polydisperse index (PDI) and encapsulation efficiency (EE%) of the resultant nanocrystals. Dynamic light scattering measurements indicated that both the average particle size and PDI first declined, but then increased, with prolonged ultrasonic treatment and increase of energy intensity (Fig. 2a). This reversal trend suggested that prolonged ultrasonication with excessive power-input could potentially disrupt the nanocrystal structure and lead to aggregation of PTX-DCA NCs. Assay by high-performance liquid chromatography (HPLC) showed an inverse correlation between the EE% of DCA with the promoted ultrasonic treatment (Fig. 2d). As a result, the nanocrystal preparations were conducted at a power intensity of 250 W for a duration of 15 min.

We next examined the effects of PTX-DCA mass ratio on the nanocrystal formation by fixing the amount of PTX at 10 mg and varying DCA from 2 mg to 10 mg with 2-mg increment. The average particle size of PTX-DCA NCs declined first and then rose with the reduced ratio (Fig. 2b), whereas the EE% of DCA exhibited a steady decrease, as the mass ratio increased (Fig. 2e). Therefore, the optimal mass ratio of PTX to DCA of 5:1 was selected for next study (10 mg PTX and 2 mg DCA).

Further optimization was focused on the evaluation of different drug payload levels under the ultrasonication conditions and mass ratio specified above. The elevation of the drug payload from 1 mg to 30 mg (based on PTX) led to an increase in both particle size and PDI (Fig. 2c), but a drop in EE% (Fig. 2f). Accordingly, the mass ratio of 10 mg of PTX and 2 mg of DCA in PTX-DCA NCs was selected as optimized drug-loading.

Taken together, we concluded that the optimal protocol for preparing PTX-DCA NCs is as follows: Performing ultrasonic treatment on the formulation of 10 mg of PTX and 2 mg of DCA at a power intensity of 250 W for 15 min. Under these conditions, the average diameter and PDI of the nanoparticles were measured to be 160.48 nm and 0.153, respectively (Fig. 2g). The EE% and DL% of PTX in the formulation measured by centrifugation followed by HPLC assay were 84.00% and 44.07%, respectively, whereas DCA showed an EE% of 33.24% and DL% of 3.46%. The nanoparticles have a total drug-loading of approximately 47% (w/w), which is extremely greater than that in the conventional drug carriers often with a drug payload of 3%–5%. A previous report argued that ultrafiltration is more accurate to determine EE% in nanoparticles compared with centrifugation [22]; however, the centrifugation method has lower cost with easy handling. Consequently, we determined the EE% by centrifugation rather than ultrafiltration.

Characterization by transmission electron microscope (TEM) revealed the nanocrystals have a rod shape with a typical particle size around 160 nm (Fig. 2h), consistent with the results from dynamic light scattering data. Serum stability demonstrated that one-hour incubation resulted in approximately 20-nm growth of the nanoparticles due to the adsorption of serum proteins, whereas no significant variation was observed in the diameter 1 h later (Fig. 3a), suggesting their potential stability after intravenous administration. PXRD analysis shows crystalline PTX has a well-defined characterized peak at $2\theta = 5.54^\circ$, 9.12° and 12.54° (Fig. 3b). The PTX-BSA mixture displays similar peaks to the pure PTX, and amorphous BSA producing no diffraction peaks (Fig. 3b). Interestingly, PTX-DCA NCs with low payload (2 mg of DCA and 10 mg of PTX) exhibited an amorphous state with no defined diffraction peaks, whereas those with a 5-fold increase of payload displayed two characteristic signals at 5.44° and 12.62°. These results confirmed that the nanoparticles are mainly present as microcrystals. *In vitro* release study depicted that hybrid crystals PTX-DCA NCs enabled faster release of the hydrophobic drug, PTX, over pure PTX crystals, PTX NCs, whereas their release profiles were similar (Fig. S1 in Supporting information).

Next, fluorescence and circular dichroism (CD) spectra were used to identify the stabilization of denature BSA on the hybrid crystals. The fluorescence emission spectra of native BSA in PBS solution registered a characteristic broad band at 340 nm attributable to tryptophan residues [23]. The intensity of this band was found to decline significantly in denatured BSA (Fig. S2a in Supporting information). In the presence of PTX-DCA NCs, we observed a clear inverse correlation between the signal intensity of the 340-nm band and the drug payload (Fig. S2b in Supporting information), which might be due to fluorescence quenching of the tryptophan residues in BSA following its binding to the highly polar DCA in the nanocrystals. Curve fitting of the fluorescence data based on the Stern-Volmer equation [24] suggested that DCA led to the static fluorescence quenching of BSA and the two were connected by strong interaction ($y = 0.9604x + 0.2738$, $r = 0.9956$; Fig. S2c in Supporting information). These experimental data confirmed that the the hybrid crystals could interact with BSA and modulate its environment in a dose-dependent manner.

The conformational changes of BSA after interacting with hybrid crystals were further investigated by far- and near-UV CD spectra [25]. The spectrum of denatured BSA shows a narrow peak at 195 nm that could be attributed to its α-helices, and a broad band at 235 nm that might arise from the conversion of the α-helices to β-folds (Fig. S2d in Supporting information), leading to enhanced structural stability of the protein [26]. However, few characterized peaks are observed in the near-UV spectrum (Fig. S2e in Supporting information). This broad band in the far-UV spectrum showed a significant red-shift in the presence of hybrid crystals (Fig. S2f in Supporting information), probably indicating the

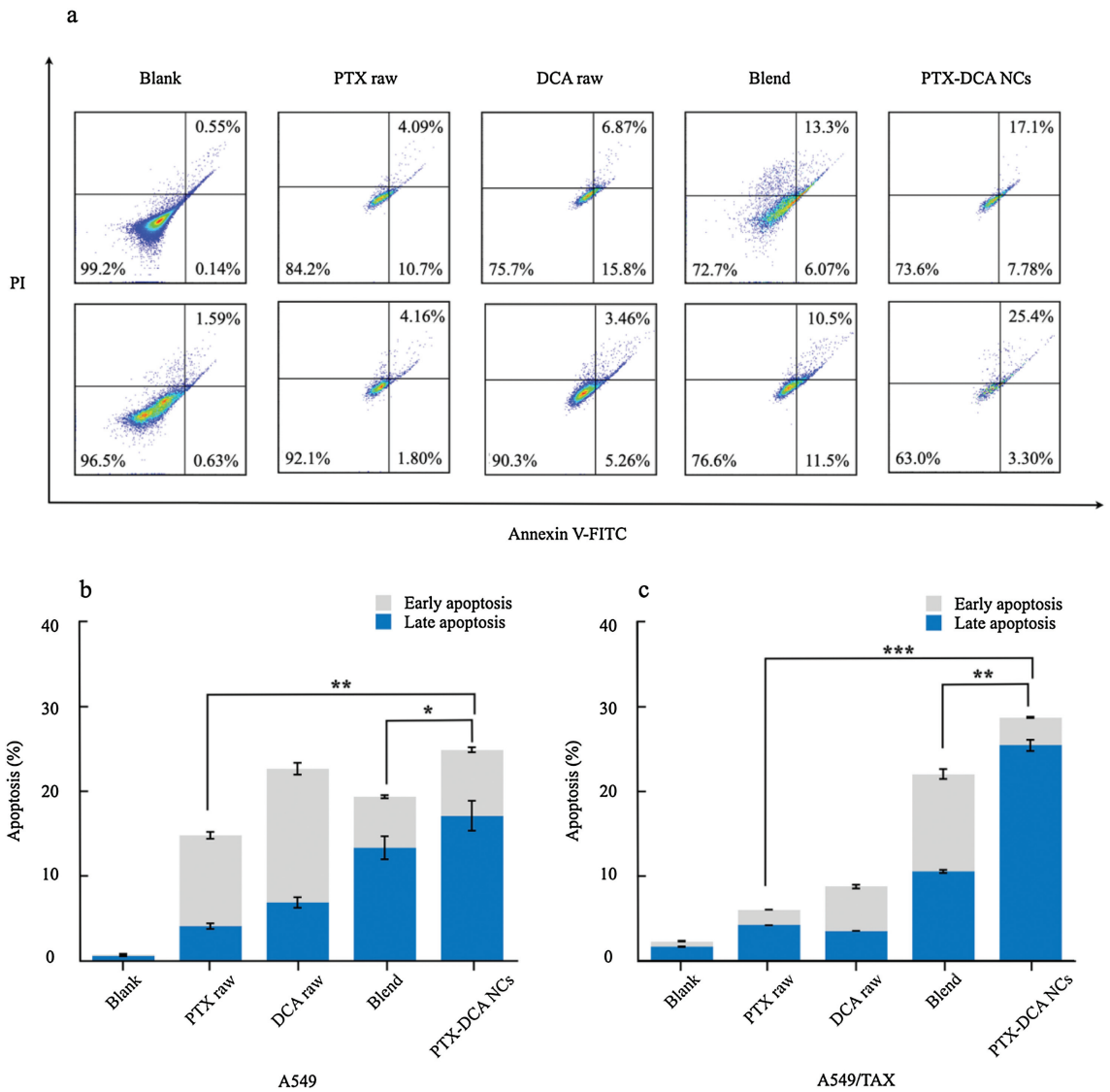

Fig. 4. Apoptosis study. (a) Flow cytometric analysis for apoptosis in A549 (top) and A549/TAX (bottom) cells after treatment with different drug formulations at a PTX or DCA concentration of 50 μg/mL for 24 h at 37 °C. Quantified apoptosis assay in (b) A549 and (c) A549/TAX cells. n = 3, $^{*}P < 0.05$, $^{**}P < 0.01$, and $^{***}P < 0.001$.

exposure of the tryptophan residues in BSA [27]. In addition, the 235-nm band was more intense with an increase of drug payloads, suggesting a concentration-dependent structural alteration of crystal-bound BSA. In the near-UV spectrum, fluorescence amplification at wavelengths of around 260 and 290 nm for the addition of the hybrid crystals is observed as well (Fig. S2g in Supporting information). Compared to native BSA, the structure of denatured BSA detected in this band does not have typical circular dichroism; while the preparation has a positive peak at 260 nm and a negative peak at 290 nm, respectively, corresponding to the β-angle and random coil structure, which may be due to the combination of protein residues and heteroatoms, resulting in its optical activity. Taken together, the observed payload-dependent conformational changes of BSA in the presence of hybrid crystals identified the interaction between the protein and the crystals and proved that the denatured BSA could serve as a stabilizer for the nanocrystals [28].

Finally, cytotoxicity *in vitro* and synergy were investigated. As depicted in Figs. S3a and b (Supporting information), all preparations exhibited dose-dependent cytotoxicity to both A549 and A549/TAX cells. Treatment with PTX-DCA NCs allowed for enhanced toxicity against the cancer cells over the incubation with one drug alone. Compared with free-drug combination, PTX-DCA NCs have generally improved cytotoxicity due to promoted cellular uptake. Especially, the combinatorial formulations, PTX-DCA NCs and free-drug combination, demonstrated higher toxicity to the PTX-resistant cells, A549/TAX cells, over A549 cells at the doses of 50 and 100 μg/mL. These results indicated that DCA is able to increase the sensitivity of cancer cells, in particular the drug-resistant cells, to the chemotherapeutic drug PTX.

To evaluate the synergy between PTX and DCA, the combination index (CI) and dose reduction index (DRI) were calculated at IC_{50} according to the cytotoxicity. As depicted in Figs. S3c and d (Supporting information), all determined CI are less than 1, indicating the synergistic effects. Also, the CI values from other ICs are lower than 1 and further demonstrated the rationality to combinatorically use the two drugs. Furthermore, the DRIs of PTX-DCA NCs for the two cell lines are greater than that from the free-drug combination (Figs. S3e and f in Supporting information).

Particularly, PTX-DCA NCs displayed improved increment of DRI for the drug-resistant cells over that for A549 cells. In addition, the CIs from IC_{50}, IC_{65}, IC_{75} and IC_{90} in the drug-resistant cells are less than that in A549 cells.

To further study the anti-tumor activity *in vitro*, examination of apoptosis in A549 cells and A549/TAX cells was performed. The free-drug combination induced apoptosis with higher efficacy than PTX or DCA alone (Fig. 4). Importantly, PTX-DCA NCs demonstrated promoted ability to kill the cancer cells over the free-drug combination. Again, PTX-DCA NCs exhibited improved potency to induce apoptosis in the drug-resistant cells over A549 cells. These results indicated that PTX and DCA have synergistic effect to kill cancer cells, especially PTX-resistant cells, and formulating them into hybrid crystals confers improved synergy.

In this study, we demonstrated that *via* a cocrystalization-like approach a hydrophilic drug can be loaded into nanocrystals of an insoluble drug and form hybrid crystals for codelivery. Our previous reports revealed that the cocrystalization-like strategy facilitated codelivery of two insoluble drugs [12,13]. Overall, the nanocrystals of a hydrophobic drug are effective to encapsulate both hydrophobic and hydrophilic active compounds acting as promising "carriers" for codelivery considering their extremely high drug-loading ability. Using the present platform, codelivery of PTX and DCA demonstrated synergy in killing cancer cells, especially PTX-resistant cells.

Declaration of competing interest

The authors report no declarations of interest.

Acknowledgments

This study was supported by the National Natural Science Foundation of China (Nos. 81872823, 81871477 and 82073782), the Double First-Class (CPU2018PZQ13, China) of the China Pharmaceutical University, the Shanghai Science and Technology Committee (No. 19430741500), and the Key Laboratory of Modern Chinese Medicine Preparation of Ministry of Education of Jiangxi University of Traditional Chinese Medicine, China (No. TCM-201905).

Appendix A. Supplementary data

Supplementary material related to this article can be found, in the online version, at doi: https://doi.org/10.1016/j.cclet.2021.03.085.

References

[1] J.M. Stewart, B.G. Keselowsky, Adv. Drug Deliv. Rev. 114 (2017) 161–174.
[2] W. He, X. Xing, X. Wang, et al., Adv. Funct. Mater. 30 (2020) 1910566.
[3] K. Zhang, P.P. Yang, J.P. Zhang, et al., Chin. Chem. Lett. 28 (2017) 1808–1816.
[4] H. He, Y. Lu, J. Qi, et al., Acta Pharm. Sin. B 9 (2019) 36–48.
[5] Y. Zhu, X. Yu, S.D. Thamphiwatana, et al., Acta Pharm. Sin. B 10 (2020) 2054–2074.
[6] I. Zoya, H. He, L. Wang, et al., Chin. Chem. Lett. 32 (2021) 1545–1549.
[7] C. Teng, C. Lin, F. Huang, et al., Acta Pharm. Sin. B 10 (2020) 1521–1533.
[8] J. Li, D.J. Burgess, Acta Pharm. Sin. B 10 (2020) 2110–2124.
[9] Y. Lu, Y. Li, W. Wu, Acta Pharm. Sin. B 6 (2016) 106–113.
[10] R. Yang, T. Zhang, J. Yu, et al., Asian J. Pharm. Sci. 14 (2019) 321–328.
[11] Y. Lu, Y. Lv, T. Li, Adv. Drug Deliv. Rev. 143 (2019) 115–133.
[12] I.S. Mohammad, W. He, L. Yin, Pharm. Res. 35 (2018) 77.
[13] I.S. Mohammad, C. Teng, B. Chaurasiya, et al., Int. J. Pharm. 557 (2019) 304–313.
[14] B. Kim, C. Lee, E.S. Lee, et al., Asian J. Pharm. Sci. 11 (2016) 708–714.
[15] D.R. Kohler, B.R. Goldspiel, J. Human Pharmacol. Drug Ther. 14 (1994) 3–34.
[16] J.L. Roh, J.Y. Park, E.H. Kim, et al., Cancer Lett. 371 (2016) 20–29.
[17] F. Gong, X. Peng, Y. Sang, et al., Cell Death Dis. 4 (2013) 913-913.
[18] I.A. Seliem, S.S. Panda, A.S. Girgis, et al., Chem. Biol. Drug Des. 95 (2020) 248–259.
[19] A. Kumar, S. Kant, S.M. Singh, Toxicol. Appl. Pharmacol. 273 (2013) 196–208.
[20] L. Zhou, L. Liu, W. Chai, et al., Onco. Target. Ther. 12 (2019) 1729–1739.
[21] R.K. Pathak, S. Marrache, D.A. Harn, S. Dhar, ACS Chem. Biol. 9 (2014) 1178–1187.
[22] Y. Lv, H. He, J. Qi, et al., Int. J. Pharm. 547 (2018) 395–403.
[23] N. Chadborn, J. Bryant, A.J. Bain, P. O'Shea, Biophy. J. 76 (1999) 2198.
[24] G.H. Wu, J. Wang, J.L. Chen, et al., Spectrosc. Spect. Anal. 28 (2008) 913–916.
[25] A. Toumadje, S.W. Alcorn, W.C. Johnson Jr., Anal. Biochem. 200 (1992) 321–331.
[26] S.M. Kelly, T.J. Jess, N.C. Price, Biochim. Biophys. Acta 1751 (2005) 119–139.
[27] K. Park, A. Perczel, G.D. Fasman, Protein Sci. 1 (1992) 1032–1049.
[28] M.D. Hays, D.K. Ryan, S. Pennell, Anal. Chem. 76 (2004) 848–854.